Hindawi

Research Article

Bayesian Regularization Backpropagation Neural Network for Glass Beams in Lateral–Torsional Buckling

Saddam Hussain ,[1] **Chiara Bedon** ,[2] **Gaurav Kumar** ,[1] **and Zaheer Ahmed**[3]

[1]*Graduate School of Engineering, Kyushu Institute of Technology, Kitakyushu, Fukuoka 804-8550, Japan*
[2]*Department of Engineering and Architecture, University of Trieste, Via Valerio 6/1, 34127, Trieste, Italy*
[3]*Department of Civil Engineering, Khawaja Fareed University of Engineering and Information Technology, 64200, Rahim Yar Khan, Pakistan*

Correspondence should be addressed to Chiara Bedon; chiara.bedon@dia.units.it

The lateral–torsional buckling (LTB) performance assessment of laminated glass (LG) beams is a remarkably critical issue because—among others—it can involve major consequences in terms of structural safety. Knowledge of LTB load-bearing capacity (in terms of critical buckling load F_{cr} and corresponding lateral displacement d_{LT}), in this regard, is, thus, a primary step for more elaborated design considerations. The present study examines how machine learning (ML) techniques can be used to predict the response of laterally unrestrained LG beams in LTB. The potential and accuracy of artificial neural networks (ANN), based on ML methods, are addressed based on validation toward literature data. In particular, to detect the best-performing data-driven ML model, the load-bearing capacity of LG beams (i.e., F_{cr} and d_{LT}) is set as output response, while geometric properties (length, width, thickness) and material features (for glass and interlayers) are used as input variables. A major advantage is taken from a literature database of 540 experiments and simulations carried out on two-ply LG beams in LTB setup. To determine the best-performing ANN model, different strategies are considered and compared. Additionally, the Bayesian regularization backpropagation (trainbr) algorithm is used to optimize the input–output relationship accuracy. The suitability of present modeling strategy for LG beams in LTB is quantitatively discussed based on error and performance trends.

1. Introduction

Soda–lime glass is increasingly used as structural material for load-bearing components in buildings and constructed facilities [1]. In this regard, it is widely known that specific modeling techniques and verification methods are required to analyze and maximize the robustness, ultimate resistance, serviceability, and stability of glass members, which are typically made of a rather brittle/vulnerable material [2], but are indeed expected to ensure safe and efficient load-bearing structural performances (Figure 1). For this reason, especially in the last two decades, a wide set of literature studies have been carried out to improve and support the structural analysis and design of glass members or systems under various loading and boundary configurations of technical significance, such as columns, beams, plates in compression or shear [3–6], etc. Regardless the specific loading and

boundary configuration and the intrinsic brittleness of glass material, a major attention goes to the design of laminated glass (LG) because the thermoplastic polymers commonly used to bond the glass sheets together are significantly temperature and load–time sensitive [2].

The present investigation specifically focuses on the buckling behavior assessment and on the load-bearing capacity prediction of LG members with beam-like structural function [7–12]. Among various relevant buckling collapse mechanisms for glass members [13–15], the attention of current study is given to unrestrained LG beams in lateral–torsional buckling (LTB), which is known to represent a possible condition of sudden and premature failure. Differing from LG beams with continuous adhesive [16–18] or discrete mechanical [19] lateral restraints, unrestrained LG beams are in fact associated to limited load-bearing capacity. For this reason, several analytical models have been elaborated in the years to capture and

FIGURE 1: Glass canopy in Tokyo, Japan (© 2023 Rafael Vinoly Architects).

predict their LTB performance [20–23]. It was, thus, shown that the critical buckling load of LG beams in LTB can be roughly predicted based on simplified estimates in which the secant–stiffness moduli for bonding interlayers is taken into account, in comparison to more refined, time-consuming but also more accurate viscoelastic finite element (FE) numerical simulations [24, 25].

The concepts of artificial intelligence (AI), machine learning (ML), and artificial neural networks (ANN) continuously spread in the industrial and research sectors. Many applications can be found for solving problems in civil and structural engineering [26], for example, to support the estimation of material properties and load-bearing parameters for a multitude of structural members and systems [27–29]. In terms of load-bearing capacity of constructional members, AI is particularly advantageous toward expensive campaigns experimental and simulation studies, especially for composite systems whose performance is based on the mechanical interaction of different materials [30–33].

The present investigation, in this regard, demonstrates how AI could be efficiently used for glass engineering applications and in particular for the specific issue of LTB performance assessment. To this aim, a database of 540 trials is taken into account from literature, and both the critical load F_{cr} and lateral displacement d_{LT} are investigated for several LG beam arrangements. A feedforward perceptron ANN model [34] is trained to generalize the output (F_{cr} and d_{LT}) for two input parameters, over the prescribed ranges. Trial and error approach is used to identify the optimal network architecture. The presented results, more in detail, show that a two-layer configuration with 10–14 neurons in the hidden layer and the tansig function performs the best, compared to other options, and can efficiently support the LTB design of LG members.

To note that the current study may possibly contribute to the development of new reliable analytical models for the design and verification of glass structures, given that various loading and boundary configurations of practical interest could be efficiently taken into account in the choosen ANN modeling strategy.

2. LTB Background and ANN Modeling Steps

2.1. Mechanical Behavior in LTB. A typical LG beam, as shown in Figure 2(a), consists of minimum two glass sheets bonded by a thermoplastic film (commonly poly (vinyl butyral) or SentryGlas). Depending on the bond shear stiffness that the interlayer can offer, the glass components can mechanically interact and contribute to the critical buckling load F_{cr} of the composite LG section. For a given LG beam in LTB setup, as far as the interlayer is stiff, the torsional stiffness of the LG section increases, and this minimizes the lateral displacement d_{LT} at midspan, under the imposed load. Besides, practical configurations of LG members can be hardly associated to a "rigid" bond condition [24, 25]. The experimental setup schematized in Figure 2(b), in this regard, was used in [24, 25] to study the LTB capacity of two-ply LG beams subjected to concentrated midspan load F, which was monotonically increased until buckling collapse. The LG beam samples were characterized by:

(i) Glass thicknesses $t_1 = t_2$ equal to 4, 10, or 19 mm, respectively.

(ii) Length L_0 comprised between 1,000 and 6,000 mm (with step increment of 1,000 mm).

(iii) Width h in the range of 120–300 mm, thus resulting in a length-to-width ratio L_0/h equals to 8, 10, 12, 15, 19, or 25, respectively.

(iv) Isotropic, elastic material properties for glass (with Young's modulus $E = 70$ GPa, shear modulus $G = 28.45$ GPa, and Poisson's ratio $n = 0.23$).

(v) A bonding interlayer with thickness t_{int}, variable shear modulus G_{int} (based on secant–stiffness equivalent approach), and Poisson's ratio $n_{int} = 0.49$.

An extended analytical and FE numerical parametric analysis was, thus, also carried out to assess the experimental evidences in terms of F_{cr}, but also in terms of typical relationship between sustained load F and corresponding out-of-plane/lateral displacement d_{LT} [24, 25]. From an analytical point of view, among the available approaches, the study in [25] highlighted the rather good accuracy of modeling strategy based on the concepts of equivalent bending stiffness $EJ_{y,eff}$ and equivalent torsional stiffness GJ_t for LTB analysis of LG beams. To note that both the above stiffness terms should necessarily account for the equivalent secant stiffness G_{int} of bonding interlayer, to reduce the scatter with viscoelastic simulations [25].

2.2. Bayesian Regularization Backpropagation Neural Network. According to above literature evidences, the present research study poses the attention on major LTB results from [25] in terms of F_{cr} and d_{LT}. A modeling strategy based on four key steps, as shown in Figure 3, is taken into account. The supporting database is split into training and test sets, with an 80%–20% ratio, and the error/performance of different ML models is compared using different accuracy metrics (Table 1). Three different closed-form equation formats (M1, M2, and M3, in the following) are taken into account, based on the application of the Bayesian regularization backpropagation algorithm (trainbr) to ANN modeling (see Figure 3 and Section 3).

To note that for present study, according to step 2, as shown in Figure 3, a dataset normalization approach is
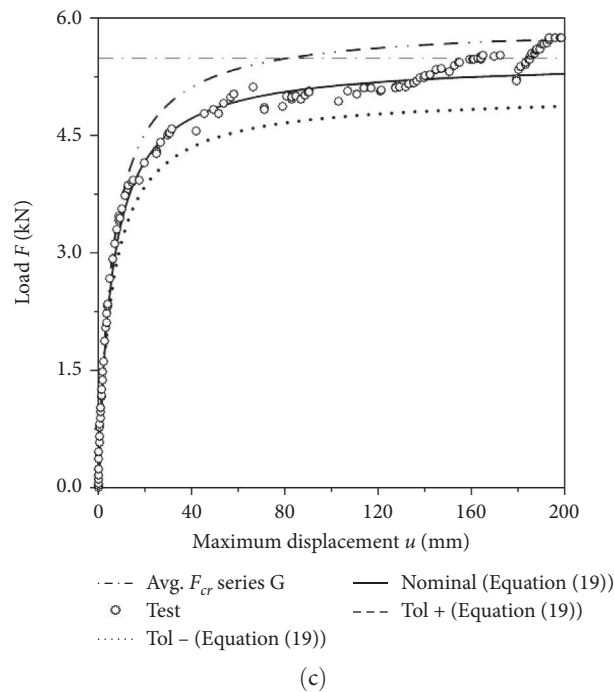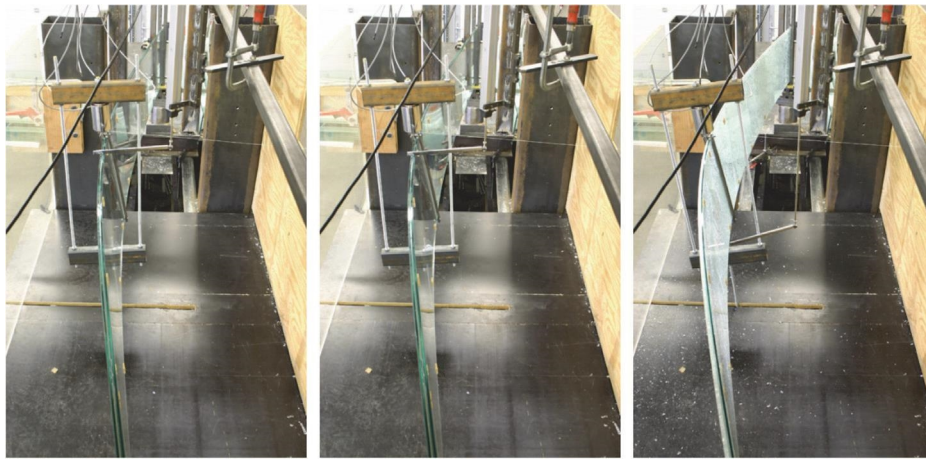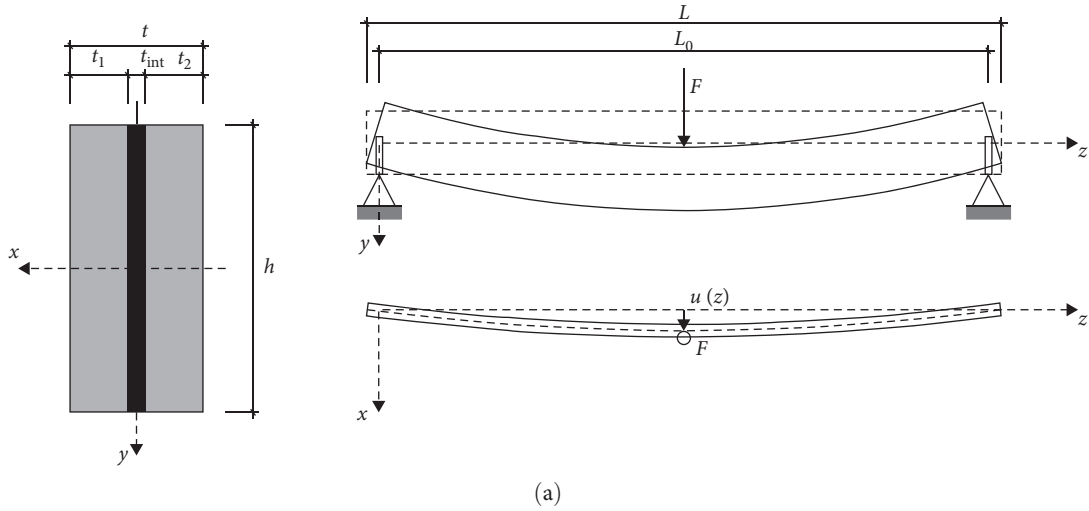
(a)

(b)

(c)

FIGURE 2: View of the typical experimental setup taken into account for LG beams in LTB under concentrated midspan load F: (a) cross-section and layout; (b) side view of experiemental stages; (c) experimentally measured load–displacement response and corresponding analytical predictions (figures (b) and (c) reproduced from [25] with permission from Elsevier©, copyright license agreement no. 5516521056620, March 2023).
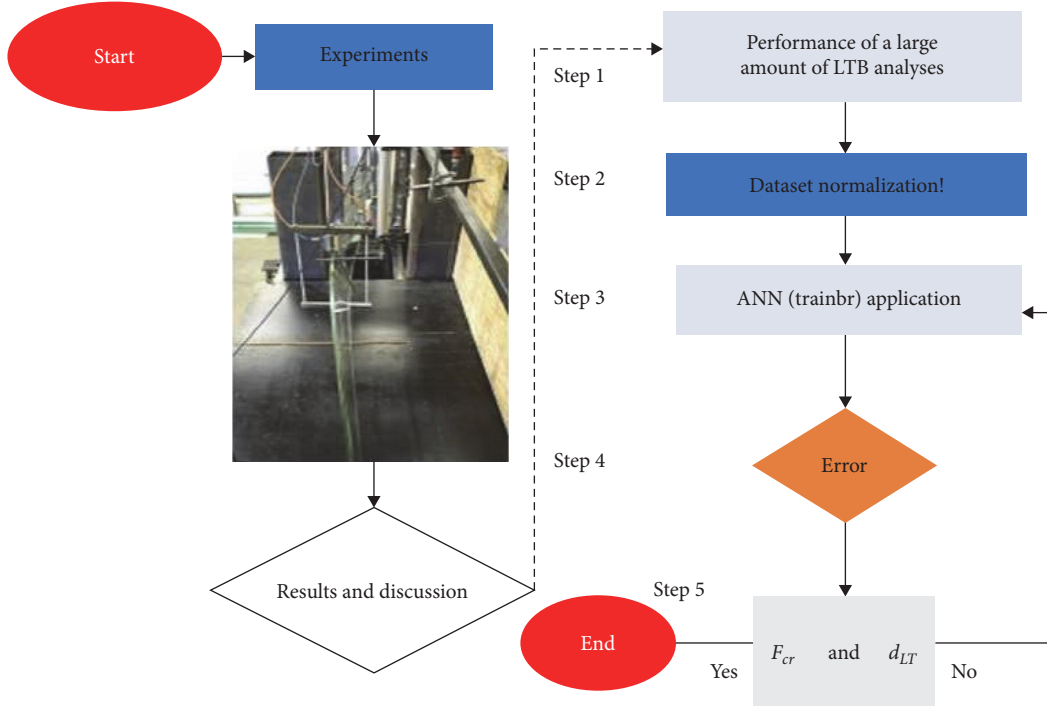
FIGURE 3: Overview of the presently adopted ANN model evaluation process.

TABLE 1: Attributes of a typical dataset.

Parameters	Information
ANN function	Bayesian regularization backpropagation (trainbr)
Number of hidden layers	2
Layer function	tansig, logsig
Output layer function	Purelin
Number of training data	540
Error criteria	Mean squared error (MSE), correlation coefficient (R)

considered to facilitate the comparison and analysis of different ML models, that is:

$$0 \leq x_i = \frac{0.8}{d_{max} - d_{min}} \cdot (d_i - d_{min}) + 0.1 \leq 1, \tag{1}$$

where d_{max} is the maximum value, d_{min} is the minimum value, and d_i is the i-th value of input and output data.

Feedforward backpropagation networks are trained in this study by using Bayesian regularization by means of the trainbr function of MATLAB® Neural Network Toolbox [35] (see step 3, as shown in Figure 3). It represents a variant of the conventional backpropagation method [36], which accelerates learning by using existing variables with information on the network parameters. The regularization settings, network structure, and training data are all inputs [37]. The trained network is subsequently given back and can be used to make predictions. The advantage of trainbr function is to reduce overfitting and enhance the network generalization performance, making it beneficial when conventional backpropagation procedures are not efficient.

For present investigation, various neural network configurations were preliminary studied. ANN, as known, is made of a huge number of neurons and interconnections. According to the structure of connections, they are classified in feedforward or recurrent. Feedforward networks have one-way connections from the input to the output layer. They are mostly (and often successfully) used for prediction and nonlinear function fitting, and many literature applications are focused on the analysis and design of constructional elements and systems [38–45]. Each neuron output is determined by:

$$a(n) = f\left(\sum_{i=1}^{n} M_i V_i + b\right), \tag{2}$$

where for present study, M_i represents F_{cr} and d_{LT}, V_i is the input vector, and b is the bias. The activation function in the hidden layer, usually tangent sigmoid based, is given by:
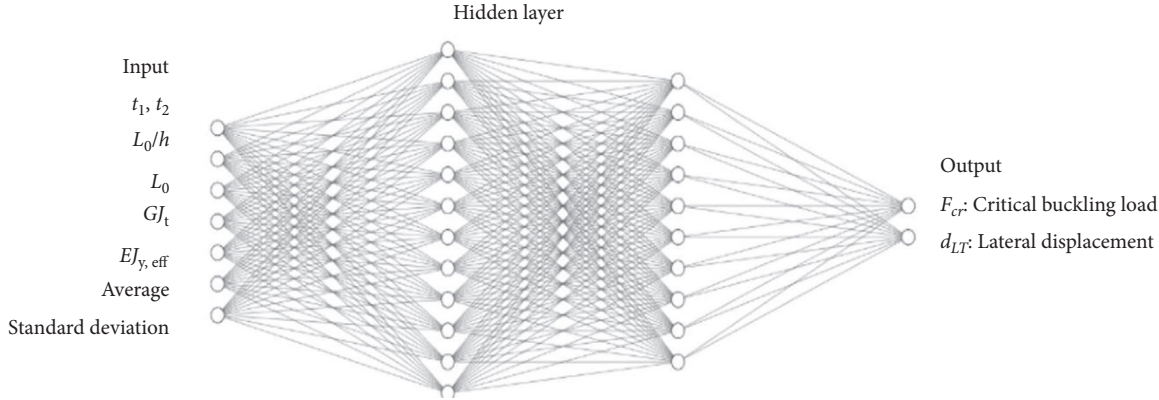
FIGURE 4: ANN multilayer model of input and output.

$$f(n) = \frac{1}{1 + e^{-n}}. \qquad (3)$$

In the specific study, a selection of length/width ratios (L_0/h) and glass thicknesses (t_1, t_2) for two-ply LG beams as in Section 2.1 is used as input layer parameters, and ANN predictions are discussed in terms of critical buckling load (F_{cr}) and corresponding lateral displacement (d_{LT}).

2.3. ANN Model Performance Assessment. For similar applications, from a mathematical point of view, one of crucial selection criteria that significantly affect the prediction outcomes is the number of neurons in the buried layer. Initially, a random number of neurons was considered to start training. Figure 4 schematically depicts the input layer, the hidden layer, and output layer. The dataset of 540 configurations was randomly divided into training (80%) and testing (20%) data, in the proportions 7 : (10–14) : (6–14) : 2. To ensure that the chosen data could be able to cover a multitude of practical configurations for LTB behavior assessment of two-ply LG beams, the recurrence of similar combinations was avoided. As shown in Figures 3 and 4, it is to note that once the network error is computed during training, the weights are modified, and the next iteration begins.

Both mean squared error (*MSE*) and correlation coefficient (*R*) were preliminary selected as evaluation criteria (step 4, as shown in Figure 3). *MSE* was determined as reported in Equation (4) and considered as the performance metric for training:

$$MSE = \frac{\left(\sum_{i=1}^{n} d_i + d_0\right)}{n}, \qquad (4)$$

where in Equation (4), d_i and d_0 represent the input and output data. The used MSE value was set as 0.001, while iterations were considered to possibly occur up to a maximum of 1.

Once all data were considered, the extra correlation coefficient *R* was taken into account to quantify the accuracy of ANN model to match the reference experiments. The correlation coefficient *R*, most importantly, reveals how much of response volatility the independent variable is able to account for, that is:

$$R = \frac{\sum xy - (\sum x)(y)}{\sqrt{\left[n\sum_x 2 - (\sum x)^2\right]\left[n\sum_y 2 - (\sum y)^2\right]}}. \qquad (5)$$

3. Discussion of Results

3.1. Trained ANN. The performance graph, which displays the fluctuation of MSE based on Equation (4) as a function of training stages, is one of the most significant indices illustrating the training status of an ANN. Figure 5, in this regard, shows the F_{cr} and d_{LT} performance for the examined LG beams in LTB. It compares the training iteration on the horizontal axis to the corresponding *MSE* on the vertical axis (epoch).

It can be seen that the *MSE* of network is maximum during the first training phase, when random critical buckling load F_{cr} (and the corresponding d_{LT}) are estimated, but it progressively decreases throughout multiple training rounds. The minimum *MSE* for training models M1, M2, and M3 is also shown in Figure 6 and appears significantly lower at the stop iteration. This confirms that untrained fresh points have higher *MSE* rate than trained points, and this is the most efficient result of early-stop technique for preventing overlearning.

A summary of error values for different training models (M1, M2, and M3) is also reported in Table 2, in terms of correlation coefficient *R*. It is possible to see that *R* tends to 0.83818 at best, which suggests some possible limits of developed model/layers. The reason of such a result can be justified by the large number of irregularities in reference experimental data, which is rather typical in structural glass testing (i.e., due to variability in material properties, small imperfections, tolerances, etc.).

For present investigation, this condition resulted—as it can be seen from the examples, as shown in Figure 7—in a rather unstable *R* value. This can be fixed by removing the outliers from reference dataset. However, the original planning choice was to use the whole dataset as a reference, irregularities included, in order to obtain a more generalized ANN model, able to incorporate all the irregularities and variabilities of input experimental data, and, thus, to account for intrinsic uncertainties of structural glass design.
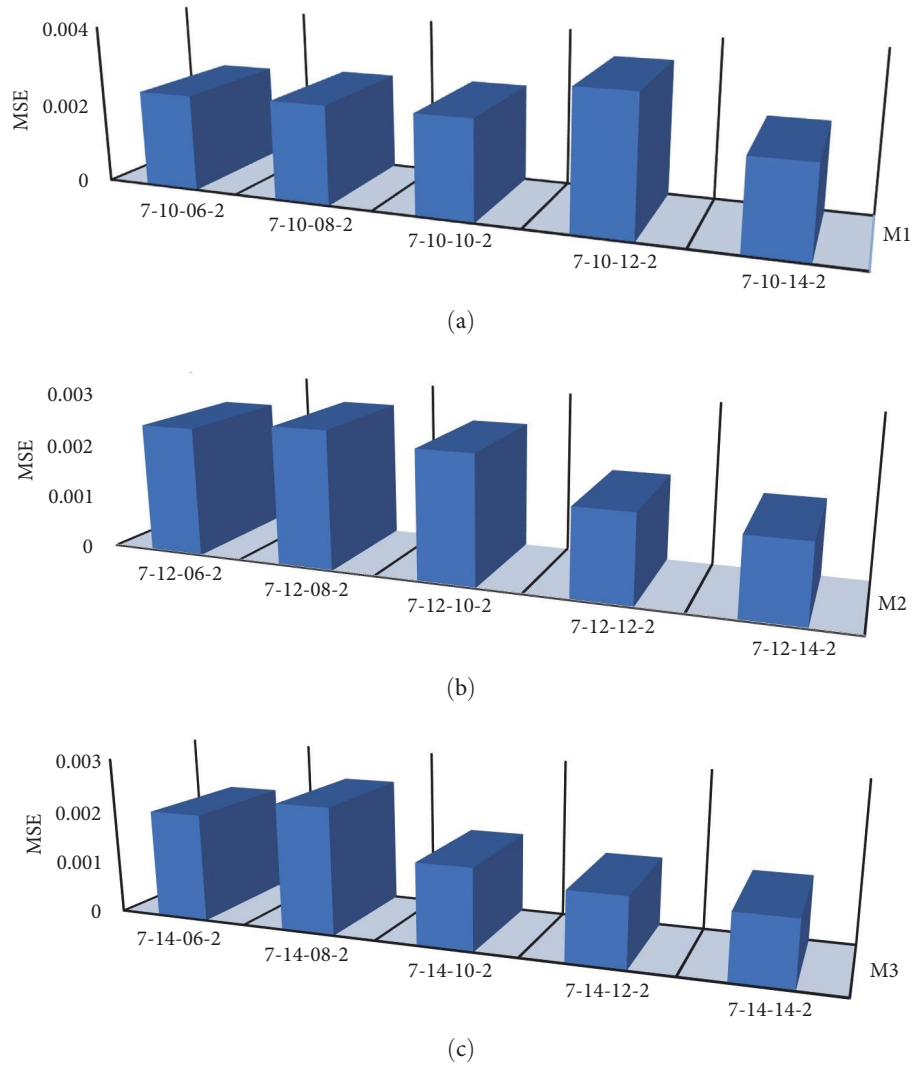
(a)

(b)

(c)

FIGURE 5: Comparison of mean squared error (MSE) values for different training stages, based on models (a) M1, (b) M2, and (c) M3 models (MATLAB).
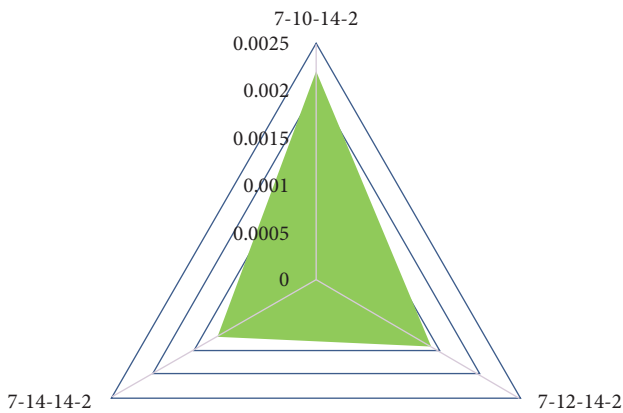

FIGURE 6: Comparison of lowest error value for training models M1, M2, and M3 (MATLAB).

Figure 8 shows the correspondence between actual network outputs and goal values. The circle represents the ideal stop time for the best performance, which has the lowest

MSE across all iterations. The network with the least MSE is chosen as best solution to estimate F_{cr} and d_{LT} for every combination of inputs, given that 10 distinct ANNs were utilized for each training scheme.

In this regard, many other performance indicators should be taken into account to assess the accuracy of developed ANN models (Figure 9). Possible markers for determining the ANN training state include, for example, data regression diagrams in terms of correlation coefficient (Figure 10).

Of course, an ideal ANN model should possibly have the same output as target value, and in this optimal condition, both the correlation coefficient R value and slope should be equal to 1, with the corresponding bias equal to 0. In the presently proposed graphs (see an example, as shown in Figure 10), it can be noted that the slope of regression is not equal to 1, but—based on intrinsic uncertainties commented, as shown in Figure 7—suggests a good potential and accuracy of proposed ANN modeling strategy. It can be, hence, deduced that current network output results have

TABLE 2: Comparison of calculated error values from different training models.

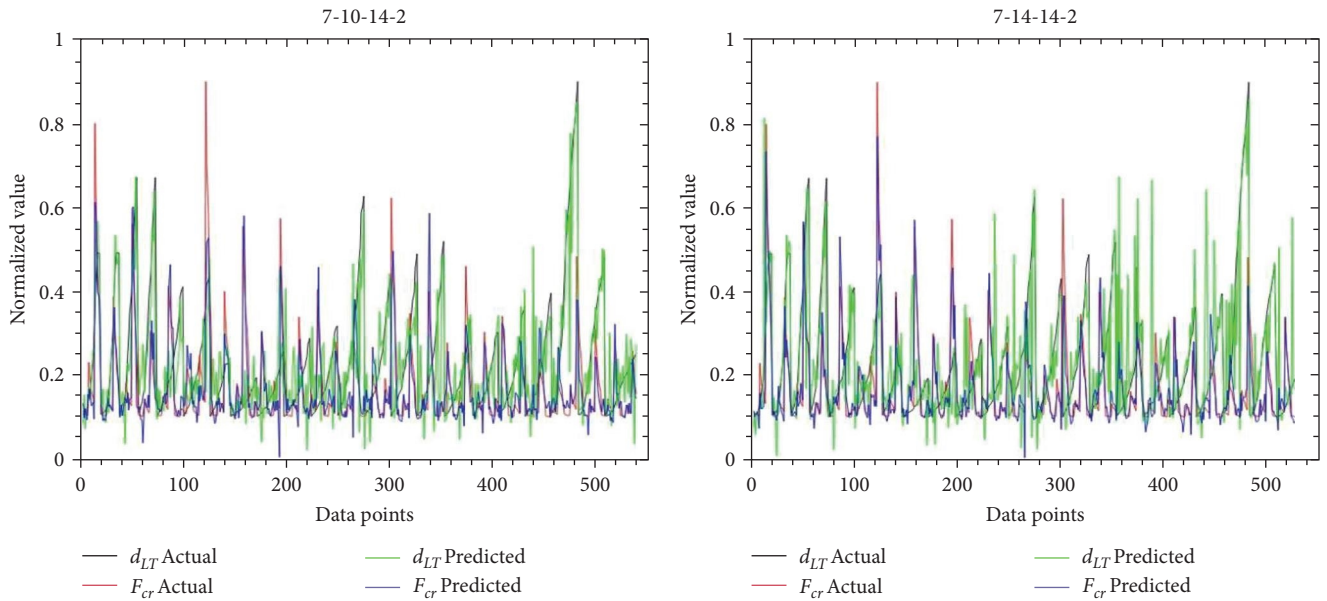| Model/layers | R (Equation (5)) | Model/layers | R (Equation (5)) | Model/layers | R (Equation (5)) |
	M1		M2		M3
7-10-06-2	0.75909	7-12-06-2	0.66017	7-14-06-2	0.6815
7-10-08-2	0.76978	7-12-08-2	0.79352	7-14-08-2	0.79156
7-10-10-2	0.73444	7-12-10-2	0.73949	7-14-10-2	0.83818
7-10-12-2	0.71817	7-12-12-2	0.7873	7-14-12-2	0.73447
7-10-14-2	0.67867	7-12-14-2	0.68073	7-14-14-2	0.75961

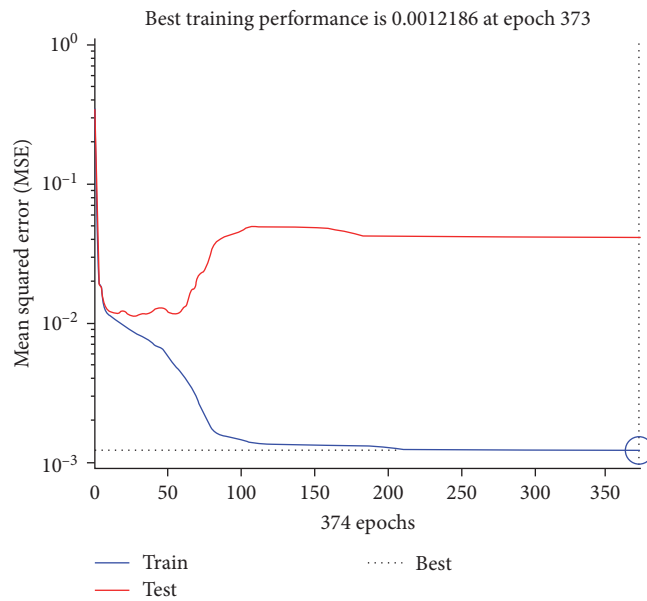FIGURE 7: Prediction of experimental values using two of the best selected ANN models.

FIGURE 8: Output performance plot for critical buckling load F_{cr} and lateral displacement d_{LT}.
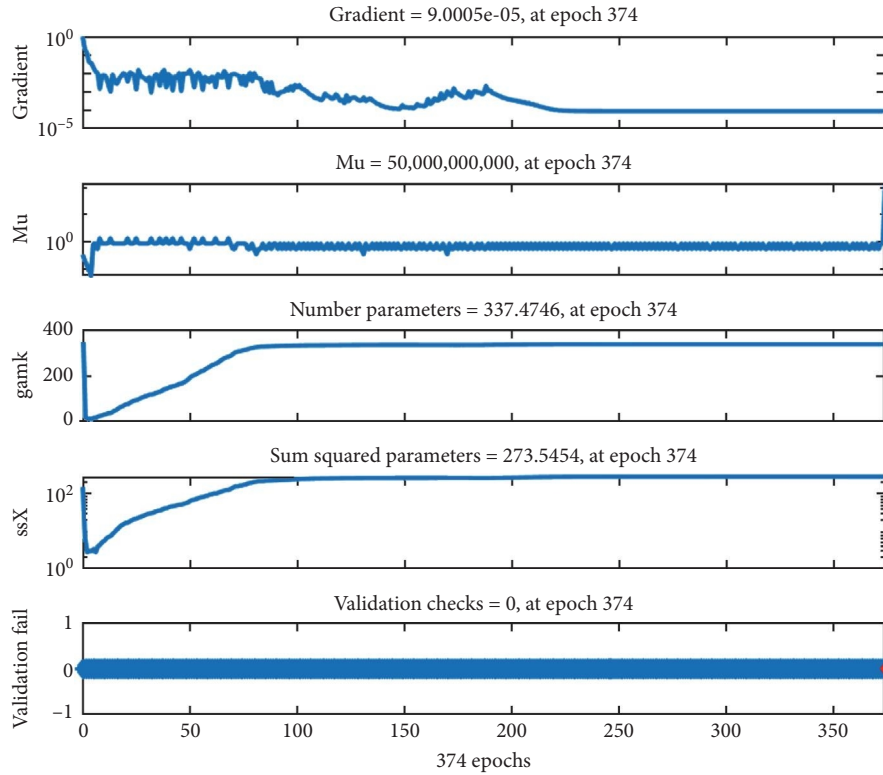
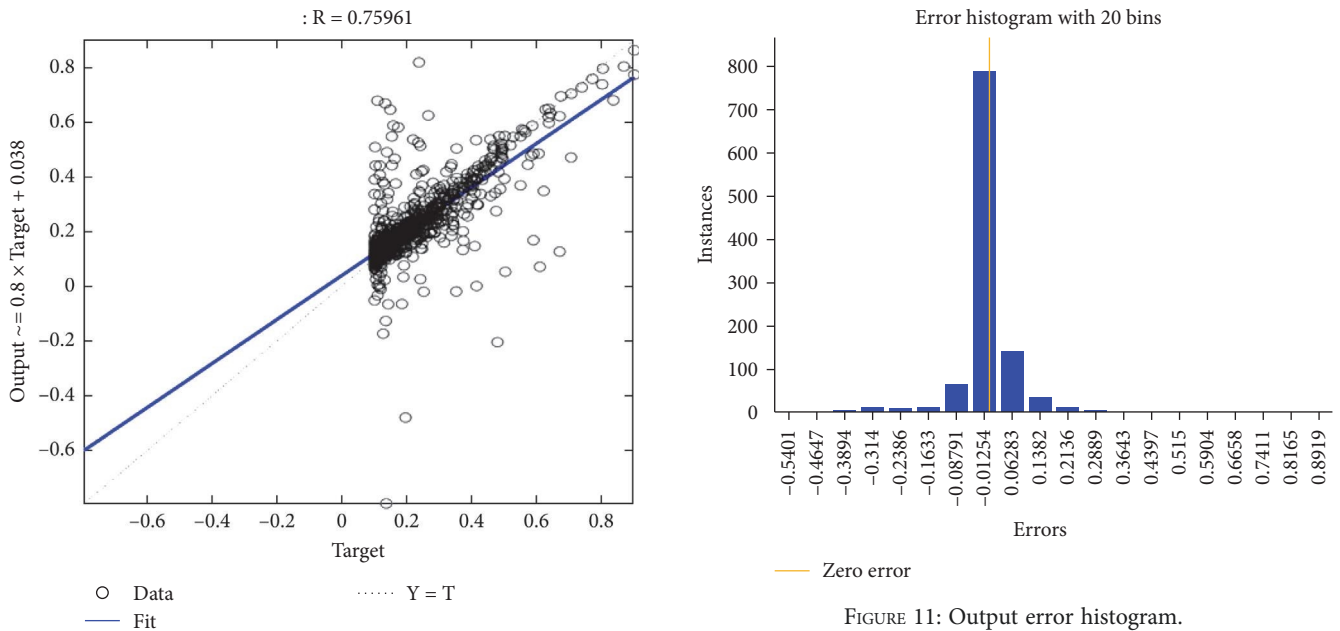FIGURE 9: Output training state parameters for critical buckling load F_{cr} and lateral displacement d_{LT}.

FIGURE 10: Output regression diagram for critical buckling load F_{cr} and lateral displacement d_{LT}.

FIGURE 11: Output error histogram.

satisfactory accuracy and are sufficiently close to target values. Moreover, the scattering style of points is at a minimum level, and all the points are located on the plane bisector. To note, as also commented in Table 2, that the presented error rate for trained ANNs is generally low, and

this result further confirms the potential of presented modeling strategy, but at the same time emphasizes the complexity and intrinsic uncertainty of structural glass performance assessment.

As shown in Figure 11, finally, error value histograms represent another crucial indicator of a well-trained ANN. The number of mistakes (frequency) in various error margins is herein reported as bar chart. The more near-zero

frequencies, or counts of mistakes, are depicted on the vertical axis as a function of various error margin values on the horizontal axis, the more accurate the ANN is. The zero-error line is also emphasized in orange. To note that the majority of bins with a high frequency of mistakes are shown to cluster around this line, which is a further conclusive evidence of a good training technique selection and a successful application of ANN modeling.

As a major outcome of present investigation, by using the trainbr technique, a well-trained two-layer ANN was produced with 10 neurons in the inner layer and based on tansig function. The calculated MSE value for predicting the critical buckling load F_{cr} and the lateral displacement d_{LT} of two-ply LG beams in LTB was measured as 0.0012186, with an associated correlation coefficient R of 0.78961.

In this sense, further investigations will be undertaken to further assess the potential of ANN tools for efficient structural design support in glass load-bearing members for constructions.

4. Conclusions

Glass members are used for structural and load-bearing applications, where they are safely design in mechanical terms to resist ordinary design actions. In support of efficient mechanical design, practical formulations in use are often developed and calibrated with the support of extensive and often complex/cost-consuming experimental tests. In this regard, the use of ANN can offer robust support. This investigation focused on the LTB performance of laterally unrestrained, two-ply LG beams. A major attention was spent for the prediction of their critical buckling load F_{cr} and corresponding out-of-plane/lateral displacement d_{LT}, which both represent crucial parameters for stability prevention and LTB verification. A major advantage was taken, through the numerical analysis, from a database of literature comprising 540 different configurations of technical interest.

The Bayesian regularization backpropagation (trainbr) algorithm was used to calibrate and optimize the accuracy of ANN model input–output relationships, by taking into account various possibilities. Most importantly, using literature data, an ANN was trained to generalize the output for two input parameters over the prescribed ranges. For this reason, a feedforward ANN was utilized, which was characterized by two outputs (F_{cr} and d_{LT}) and six input parameters (i.e., LG beam geometry). Trial and error approach led to the discovery of the optimum ANN structure, which consisted of two layers with 10 neurons in the hidden layer and the tansig function. Also, 15 training models were employed to examine the impact of trainbr training algorithms on the effectiveness of output prediction. At every test fraction combination, the trained ANN was used to serve as prediction function in terms of F_{cr} and d_{LT}.

Overall, the rather good accuracy and potential of ANN modeling and its suitability for determining the load-bearing capacity of two-ply LG beams in LTB, as well as the competence of the employed training procedures, were demonstrated by variation error diagrams and histograms. In this sense, it is expected that the same modeling strategy could be further extended in support of many practical applications of interest for the structural glass optimization in buildings, including several layouts, material properties, and even loading/boundary configurations.

Data Availability

The data supporting the research study will be shared upon request.

Conflicts of Interest

The authors declare that they have no conflicts of interest.

Authors' Contributions

All authors contributed to formal analysis, software, writing, and editing the submitted manuscript.

Acknowledgments

References

[1] N. Emami, "Glass structures, from theory to practice," in *Structures and Architecture: New Concepts, Applications and Challenges*, P. J. Cruz, Ed., pp. 305–311, CRC Press, London, 1st edition, 2013.

[2] M. Feldmann, M. Laurs, J. Belis et al., "The new CEN/TS 19100: design of glass structures," *Glass Structures & Engineering*, 2023.

[3] S. Hussain, P.-S. Chen, N. Koizumi et al., "Feasibility of computational intelligent techniques for the estimation of spring constant at joint of structural glass plates: a dome-shaped glass panel structure," *Glass Structures & Engineering*, vol. 8, pp. 141–157, 2023.

[4] Y. Tian, Z. Yang, W. Chen, and X. Lu, "Pseudo static experimental study on spider-supported glass curtain walls," *Glass Structures & Engineering*, vol. 7, pp. 681–691, 2022.

[5] C. Bedon and C. Amadio, "Mechanical analysis and characterization of IGUs with different silicone sealed spacer connections—Part 1: experiments," *Glass Structures & Engineering*, vol. 5, pp. 301–325, 2020.

[6] L. Galuppi and E. Riva, "Experimental and numerical characterization of twisting response of thin glass," *Glass Structures & Engineering*, vol. 7, pp. 45–69, 2022.

[7] J. Belis, J. Depauw, D. Callewaert, D. Delincé, and R. Van Impe, "Failure mechanisms and residual capacity of annealed glass/SGP laminated beams at room temperature," *Engineering Failure Analysis*, vol. 16, no. 6, pp. 1866–1875, 2009.

[8] A. B. Ølgaard, J. H. Nielsen, and J. F. Olesen, "Design of mechanically reinforced glass beams: modelling and

experiments," *Structural Engineering International*, vol. 19, no. 2, pp. 130–136, 2009.

 [9] M. Netusil and M. Eliasova, "Design of the composite steel-glass beams with semi-rigid polymer adhesive joint," *Journal of Civil Engineering and Architecture*, vol. 6, no. 8, pp. 1059–1069, 2012.

[10] S. Jordão, M. Pinho, J. P. Martin, A. Santiago, and L. C. Neves, "Behaviour of laminated glass beams reinforced with pre-stressed cables," *Steel Construction*, vol. 7, no. 3, pp. 204–207, 2014.

[11] R. Ringli and T. Vogel, "Load-bearing behavior of spliced glass beams under bending action," *Glass Structures & Engineering*, vol. 1, pp. 61–80, 2016.

[12] O. Pešek, J. Melcher, and I. Balázs, "Experimental verification of the structural glass beam-columns strength," *IOP Conference Series: Materials Science and Engineering*, vol. 245, Article ID 032068, 2017.

[13] C. Amadio and C. Bedon, "Analytical approaches for buckling verification of in-plane loaded laminated glass columns and panels," in *Challenging Glass 3*, F. Bos, C. Louter, R. Nijsse, and F. Veer, Eds., pp. 373–386, IOS Press, 2012.

[14] C. Bedon and C. Amadio, "Buckling of flat laminated glass panels under in-plane compression or shear," *Engineering Structures*, vol. 36, pp. 185–197, 2012.

[15] C. Amadio and C. Bedon, "A buckling verification approach for monolithic and laminated glass elements under combined in-plane compression and bending," *Engineering Structures*, vol. 52, pp. 220–229, 2013.

[16] C. Bedon and C. Amadio, "Analytical and numerical assessment of the strengthening effect of structural sealant joints for the prediction of the LTB critical moment in laterally restrained glass beams," *Materials and Structures*, vol. 49, pp. 2471–2492, 2016.

[17] C. Bedon, J. Belis, and C. Amadio, "Structural assessment and lateral–torsional buckling design of glass beams restrained by continuous sealant joints," *Engineering Structures*, vol. 102, pp. 214–229, 2015.

[18] C. Bedon, "Lateral-torsional buckling (LTB) method for the design of glass fins with continuous lateral restraints at the tensioned edge," *Composite Structures*, vol. 266, Article ID 113790, 2021.

[19] D. Santo, S. Mattei, and C. Bedon, "Elastic critical moment for the lateral–torsional buckling (LTB) analysis of structural glass beams with discrete mechanical lateral restraints," *Materials*, vol. 13, no. 11, Article ID 2492, 2020.

[20] A. Luible, "Stabilität von tragelementen aus glas," Lausanne, Switzerland, Thèse EPFL 3014, Ecole Polytechnique Fédérale de Lausanne (EPFL), 2004.

[21] J. Belis, *Kipsterkte van Monolithische en Gelamineerde Glazen Liggers*, Ghent University, Ghent, Belgium, 2005.

[22] R. Kasper, *Tragverhalten von Glasträgern*, Shaker Verlag Gmbh, RWTH Aachen, Aachen, Germany, 2005.

[23] C. Amadio and C. Bedon, "Buckling of laminated glass elements in out-of-plane bending," *Engineering Structures*, vol. 32, no. 11, pp. 3780–3788, 2010.

[24] J. Belis, C. Bedon, C. Louter, C. Amadio, and R. V. Impe, "Experimental and analytical assessment of lateral torsional buckling of laminated glass beams," *Engineering Structures*, vol. 51, pp. 295–305, 2013.

[25] C. Bedon, J. Belis, and A. Luible, "Assessment of existing analytical models for the lateral torsional buckling analysis of PVB and SG laminated glass beams via viscoelastic simulations

[26] N. D. Lagaros, "Artificial neural networks applied in civil engineering," *Applied Sciences*, vol. 13, no. 2, Article ID 1131, 2023.

[27] F. Özcan, C. D. Atiş, O. Karahan, E. Uncuoğlu, and H. Tanyildizi, "Comparison of artificial neural network and fuzzy logic models for prediction of long-term compressive strength of silica fume concrete," *Advances in Engineering Software*, vol. 40, no. 9, pp. 856–863, 2009.

[28] D. V. Dao, S. H. Trinh, H.-B. Ly, and B. T. Pham, "Prediction of compressive strength of geopolymer concrete using entirely steel slag aggregates: novel hybrid artificial intelligence approaches," *Applied Sciences*, vol. 9, no. 6, Article ID 1113, 2019.

[29] S. I. Haruna, S. I. Malami, M. Adamu et al., "Compressive strength of self-compacting concrete modified with rice husk ash and calcium carbide waste modeling: a feasibility of emerging emotional intelligent model (EANN) versus traditional FFNN," *Arabian Journal for Science and Engineering*, vol. 46, pp. 11207–11222, 2021.

[30] D. R. Cassar, A. C. P. L. F. de Carvalho, and E. D. Zanotto, "Predicting glass transition temperatures using neural networks," *Acta Materialia*, vol. 159, pp. 249–256, 2018.

[31] A. H. Le, F. Ekkehard, D.-K. Thai, and C. V. Nguyen, "Simplified critical buckling load Fcr-strain model for circular steel tube confined UHPC and UHPFRC columns," *Steel and Composite Structures*, vol. 29, no. 1, pp. 125–138, 2018.

[32] A. I. Nour and E. M. Güneyisi, "Prediction model on compressive strength of recycled aggregate concrete filled steel tube columns," *Composites Part B: Engineering*, vol. 173, Article ID 106938, 2019.

[33] L.-H. Han, G.-H. Yao, Z.-B. Chen, and Q. Yu, "Experimental behaviours of steel tube confined concrete (STCC) columns," *Steel and Composite Structures*, vol. 5, no. 6, pp. 459–484, 2005.

[34] I. Flood and N. Kartam, "Neural networks in civil engineering. I: Principles and understanding," *Journal of Computing in Civil Engineering*, vol. 8, no. 2, pp. 131–148, 1994.

[35] MATLAB (R2018a), *Version 9.4 Natick*, The MathWorks Inc., Natick, MA, USA, 2018.

[36] S. Gouravaraju, R. A. Sauer, and S. S. Gautam, "Investigating the normal and tangential peeling behaviour of gecko spatulae using a coupled adhesion-friction model," *The Journal of Adhesion*, vol. 97, no. 10, pp. 952–983, 2021.

[37] S. Gouravaraju, R. A. Sauer, and S. S. Gautam, "On the presence of a critical detachment angle in gecko spatula peeling—a numerical investigation using an adhesive friction model," *The Journal of Adhesion*, vol. 97, no. 13, pp. 1234–1254, 2021.

[38] S. A. M. Davoudi and M. Naghipour, "The effect of slenderness ratio on modification of compressive strength of AISC code for composite columns (CFT) T-shaped with numerical (FEM) and experimental analysis," *Results in Materials*, vol. 9, Article ID 100124, 2021.

[39] J. Suhardjo, B. F. Spencer Jr., and M. K. Sain, "Feedback–feed-forward control of structures under seismic excitation," *Structural Safety*, vol. 8, no. 1–4, pp. 69–89, 1990.

[40] Q. Albu-Jasim and G. Papazafeiropoulos, "A neural network inverse optimization procedure for constitutive parameter identification and failure mode estimation of laterally loaded unreinforced masonry walls," *CivilEng*, vol. 2, no. 4, pp. 943–968, 2021.

[41] H. Q. Le, T. T. Truong, D. Dinh-Cong, and T. Nguyen-Thoi, "A deep feed-forward neural network for damage detection in functionally graded carbon nanotube-reinforced composite plates using modal kinetic energy," *Frontiers of Structural and Civil Engineering*, vol. 15, pp. 1453–1479, 2021.

[42] I. Faridmehr, M. Nikoo, R. Pucinotti, and C. Bedon, "Application of component-based mechanical models and artificial intelligence to bolted beam-to-column connections," *Applied Sciences*, vol. 11, no. 5, Article ID 2297, 2021.

[43] W. A. Altabey and M. Noori, "Fatigue life prediction for carbon fibre/epoxy laminate composites under spectrum loading using two different neural network architectures," *International Journal of Sustainable Materials and Structural Systems*, vol. 3, no. 1, pp. 53–78, 2017.

[44] A. G. Stamopoulos, K. I. Tserpes, and A. J. Dentsoras, "Quality assessment of porous CFRP specimens using X-ray computed tomography data and artificial neural networks," *Composite Structures*, vol. 192, no. 10, pp. 327–335, 2018.

[45] M. Gayatri Vineela, A. Dave, and P. K. Chaganti, "Artificial neural network based prediction of tensile strength of hybrid composites," *Materials Today: Proceedings*, vol. 5, no. 9, pp. 19908–19915, 2018.